Materials Science and Engineering A 394 (2005) 9–19

www.elsevier.com/locate/msea

The dependence of the β-AlFeSi to α-Al(FeMn)Si transformation kinetics in Al–Mg–Si alloys on the alloying elements

N.C.W. Kuijpers[a], F.J. Vermolen[b,*], C. Vuik[b], P.T.G. Koenis[c], K.E. Nilsen[c], S. van der Zwaag[a,d]

[a] *Netherlands Institute of Metals Research (NIMR), Postbus 5008, 2600 GA Delft, The Netherlands*
[b] *Department of Applied Mathematics, Delft University of Technology, Postbus 5031, 2600 GA Delft, The Netherlands*
[c] *BOAL BV, Postbus 75, 2678 ZH De Lier, The Netherlands*
[d] *Department of Aerospace Engineering, Delft University of Technology, Postbus 5058, 2600 GB Delft, The Netherlands*

Received 6 September 2004

Abstract

An homogenisation process is applied to as cast billets Al–Mg–Si alloys in order to improve the extrudability. During this homogenisation, plate-like β-AlFeSi phase transforms to a more rounded α-Al(FeMn)Si phase which are more favourable for the extrusion process. In this paper, the influence of the alloying elements on the rate of the intermetallic β-to-α transformation is studied. A Finite Element Model (FEM) predicts the kinetics of the β-to-α transformation for various Mn and Si concentrations. The software package Thermo-Calc is used to derive the equilibrium solubilities for various alloy compositions. These solubilities are used in the Finite Element Method as boundary conditions for the interfacial concentrations of the intermetallics. Subsequently, the results of the Finite Element Model are validated with experimental data.

Keywords: Phase transformation; Intermetallics; Aluminium alloy; Diffusion; Stefan problem

1. Introduction

The phase transformation of β-AlFeSi to α-Al(FeMn)Si is an important process during the homogenisation of as-cast AA 6xxx aluminium alloys. During this homogenisation process, at temperatures between 530 and 600 °C [1], plate-like monoclinic intermetallic β-Al_5FeSi particles transform to more globular cubic α-$Al_{12}(Fe_xMn_{(1-x)})_3Si$ particles [2–4]. This phase transformation improves the process quality of the aluminium considerably. The plate-like β-particles can lead to local crack initiation and induce surface defects on the extruded material. The more globular α-particles in the homogenised material improve the extrudability of the material and the surface quality of the extruded material [5]. Additional processes, such as the dissolution of Mg_2Si particles also occur during homogenisation. Since the Mg_2Si particles dissolve rather quickly, the β-to-α transformation kinetics determine the required minimum homogenisation time [6].

Many process parameters such as homogenisation temperature and as-cast microstructure influence the transformation rate. The influence of those parameters is described by Kuijpers et al. [7]. In this paper, the influence of alloy composition, in particular the Mn and Si concentration, on the rate of the β-to-α transformation is studied.

Of all main alloying elements in 6xxx alloys, Mn seems to have the largest influence on the transformation rate. For very low Mn levels, less than approximately 0.01 wt.%, hexagonal α_h-AlFeSi phase is the stable phase [8] and transformation rates are very low. For Mn concentrations >0.02 wt.% the cubic α-Al(FeMn)Si phase is the stable phase. In addition, the β-to-α transformation speed increases [2]. A further in-

* Corresponding author. Present address: Department of Applied Mathematical Analysis, Delft University of Technology, Mekelweg 4, Delft 2628 CD, The Netherlands. Tel.: +31 15 2787298; fax: +31 15 2787209.
E-mail address: F.J.Vermolen@ewi.tudelft.nl (F.J. Vermolen).

0921-5093/$ – see front matter © 2004 Elsevier B.V. All rights reserved.
doi:10.1016/j.msea.2004.09.073

crease of the Mn content increases the β-to-α transformation rate even more. The influence of Si is less significant than that of Mn and has been overlooked for a long time. However, recently it has been shown that an increase in Si content decreases the transformation rate [1].

However, no study has been presented yet which explains the origin of the influence of Mn and Si on the transformation speed. It is the aim of this paper to present a validated model for this dependence. We use the same Finite Element Model (FEM) as presented in [7]. This FEM applies to the β-to-α transformation in the early state up to a transformed α-fraction of approximately 50%. In addition, we use a thermodynamic database TTAL [9] of the software package Thermo-Calc to derive equilibrium solubilities for various Mn and Si alloying levels. The equilibrium solubility products at the β-interfaces thus derived are used in a multi-component particle dissolution model, described by Vermolen and Vuik [10], to obtain the interfacial concentrations of the alloying elements. Then, the interfacial concentrations are used as boundary conditions for the Finite Element calculations. In these FEM calculations geometrical parameters are used which are obtained from an experimental characterisation of the alloys. Subsequently, the results of the Finite Element Model are validated with experiments.

2. Al–Fe–Si–Mn phase diagrams

Fig. 1a shows the aluminium corner of the Al–Fe–Si phase diagram [8,11–15]. The influence of Mg, which is always present in AA 6xxx alloys, on the phase diagram is small [15], and therefore this phase diagram is a good approximation of the phase diagram of a Mn free AA 6xxx alloys. As Mn-free AA 6xxx alloys contain small amounts of Fe and Si, the phase diagram indicates that besides matrix Al only the hexagonal α_h-Al_8FeSi or the β-AlFeSi phases are stable. The other phases in Fig. 1a, such as Al_3Fe, $AlFeSi_2$ and Al_3FeSi are only stable if the alloy content deviates from the 6xxx family of alloys, e.g. for high Fe and Si contents. Note that in this Al–Fe–Si phase diagram the cubic α phase (α_c) is not present, since a minimum Mn content is required to stabilise this phase.

Fig. 1b shows an enlargement of the calculated aluminium corner of the Al–Fe–Si phase diagram at a temperature of 540 °C, showing a quantitative picture of the aluminium-rich part. This is obtained by use of the Thermo-Calc database. The graph shows that the maximum solubility of Fe in Al is considerably lower (∼0.015 wt.%) than the maximum solubility of Si (∼1 wt.%). Fig. 1b shows that high, intermediate, and low Fe/Si alloy-content ratios lead to stabilisation of the Al_3Fe, α_h and β phases, respectively. The effect of Fe/Si ratio and the Si content on the stable phases has been confirmed experimentally [1,2,15,16].

The alloy composition of 6xxx alloys is designed such that the stable intermetallic phase is the α phase. By extrapolating Fig. 1b it can be shown that for a lowly Si alloyed AA 6xxx

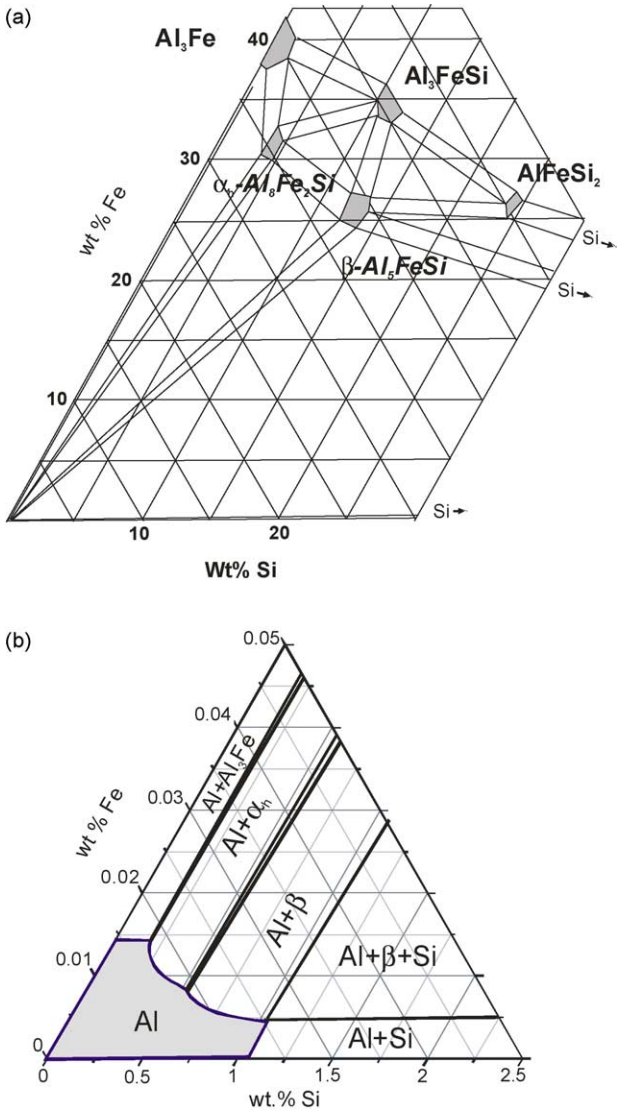

Fig. 1. (a) The Al-corner of the Al–Fe–Si phase diagram [8]. (b) Enlargement of the Al-corner of the calculated Al–Fe–Si phase diagram, as derived by Thermo-Calc for a temperature of 540 °C. Note that in this graph, the Fe-scale is enlarged.

system (e.g. 0.6 wt.%) a low Fe alloy content (∼0.20 wt.%) is required, whilst for a highly Si alloyed 6xxx system (e.g. 1.5 wt.%) a high Fe content is required (∼0.5 wt.%). In the previous phase diagram only the hexagonal α phase (α_h) was present since Mn was absent. It is also interesting to study the influence of Mn on the stabilisation of the cubic α (α_c) intermetallics. This influence is depicted in the phase diagram of Fig. 2a, which is constructed using the results of [8,17] and the Thermo-Calc package. The figure shows that the presence of some manganese stabilises the α_c phase. The Mn content of the stabilised α_c phase is highly dependent on the alloy composition, as indicated by the tie-lines. This was also found by Tibbals et al. [17]. Some authors [8,17] found some slight change in stoichiometry of the α phase as the Fe/Mn ratio changes. However, since these changes are

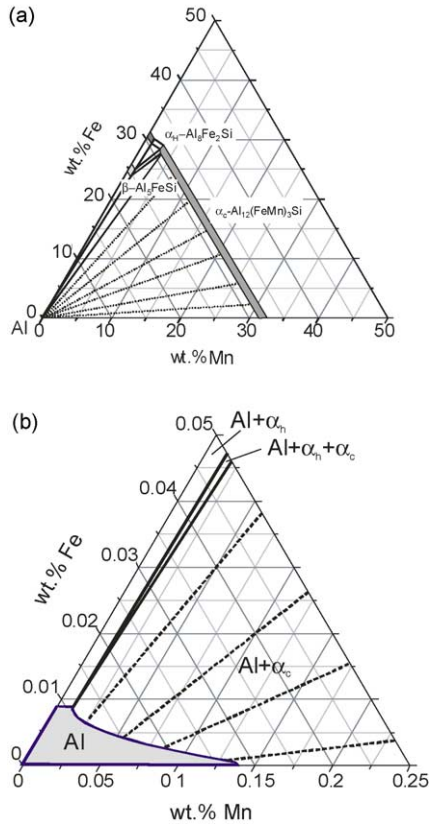

Fig. 2. (a) Projections of the Al–Fe–Mn–Si phase diagram onto the Al–Mn–Fe plane. The non-relevant intermetallic phases for 6xxx series are left away. (b) Enlargement of the Al-corner of the Al–Fe–Mn–Si phase diagram, as derived by Thermo-Calc for a fixed Si matrix concentration of 0.5 wt.% at 540 °C. Note that, in this graph, the Fe-scale is enlarged.

only small we neglect them in the presented phase diagram of Fig. 2a, and we use the $Al_{12}(Fe_xMn_{1-x})_3Si$ stoichiometry in our calculations.

Fig. 2b shows an enlargement of the aluminium corner of the phase diagram of Fig. 2a. In this graph, the Al-phase is visualised, where the β-phase is not taken into account. The figure shows again that the solubility of Fe is very small (∼0.01) compared to the solubility of Mn (∼0.15 wt.% Mn). This graph also shows that the equilibrium Fe and Mn matrix concentration of the aluminium is highly dependent on the Fe to Mn alloy ratio, as indicated by the dotted tie-lines: for a high Fe-to-Mn ratio the hexagonal α phase (α_h) is stabilised, whilst for lower Fe-to-Mn ratios the cubic α phase (α_c) is stabilised. Similar results are obtained for other Si concentrations within the AA 6xxx compositional window.

3. The model

3.1. Introduction

Since the Finite Element Model of the β-to-α transformation is already presented in detail in [7], we only give a brief introduction to this Finite Element Model. After this, a thermodynamic study is presented, showing the influence of Mn and Si levels in the alloy on the concentrations of Fe of the interfaces. These concentrations are an input in the FEM and influence the transformation speed.

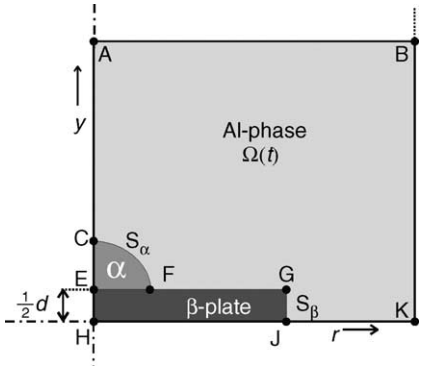

Fig. 3. The geometry of the domain of computation of an α particle on a β plate in an Al-phase. The parameters are explained in the text.

3.2. General description of Finite Element Model

Fig. 3a schematic representation of the particle and matrix as modelled in the FEM. For the model cylindrical coordinates are used where the line AH is the axis of symmetry. This geometry presents a piece of the original β-plate with one α nucleus on top of it. The FEM describes the growth of the α-particle towards the dissolving rim S_β of the β-plate. During the transformation, the thickness of the β plate remains constant. The α particle grows along the entire α/Al interface, indicated by S_α. The transformation is assumed to be diffusion controlled, and its driving force is given by the difference in chemical potential. Fe and Si diffuse from the β rim through the aluminium matrix towards the α particle. Since the diffusion speed of Fe is a few orders slower than that of Si, only the diffusional fluxes of Fe are dealt with in the model. The velocities of the moving boundaries S_α and S_β are derived by the use of the Stefan condition [18], considering the equilibrium interface concentration, and the diffusion flux at the boundary. All FEM calculations are performed using the software package SEPRAN, which has been developed at the Department of Applied Mathematics at the Delft University of Technology, The Netherlands.

Table 1 presents the model parameters used for the FEM. The Fe particle concentrations were derived by use of the densities and the stoichiometry of the α and β phases. The geometrical parameters, such as initial radius of the α particle, initial thickness, and initial diameter of the β plate were obtained experimentally at 580 °C [7]. In the FEM calculations, it is assumed that the geometrical starting parameters are not affected by the variation of the matrix content in Si and Mn level and by temperature.

Since the dimensions of the volume considered in the model is smaller than the DAS spacing we assume that the initial Si and Fe concentration is equally distributed in the matrix.

Table 1
Basic physical parameters which are used for the Finite Element Model calculations

Parameter	Symbol	Value
Diffusion pre-factor of Fe [19]	D_0	5.3×10^{-3} m^2 s^{-1}
Activation energy of diffusion of Fe [19]	Q	183.4 kJ/mol
Fe concentration in α particle [8]	c_α^p	39.9 wt.%
Fe concentration in β particle [8]	c_β^p	33.9 wt.%
Initial radius of α particle	$r_\alpha^{\text{initial}}$	0.25 μm
Thickness of β-plate	D	0.2 μm
Equivalent diameter of initial β-plate	l	1.5 μm
Cell size of aluminium matrix	l_{cell}	2.5 μm
Temperature	T	853 K (580 °C)

We assume that the matrix is initially in equilibrium with the β particle. In the FEM we do not take Mn diffusion into account, and we assume that the Mn matrix composition remains constant during time.

3.3. Thermodynamics

As demonstrated in [7] we argue that the main driving force of the transformation is the difference in chemical potential ($\Delta\mu_{\text{Fe}}$) of solute iron on the interfaces (S_α and S_β) of the phases in the aluminium alloy:

$$\Delta\mu_{\text{Fe}} = \mu_\beta^S - \mu_\alpha^S \quad (1)$$

This difference in chemical potential of the iron solute levels in the Al-phase close to the α (μ_α^S) and the β interface (μ_β^S), result in a diffusional flux of iron atoms towards the α phase. It is assumed that the interfacial reactions are fast enough to maintain local thermodynamic equilibrium concentrations at the α/Al and β/Al interface. The chemical potentials of Fe at the two interfaces depend on the solute levels of other elements, such as Si and Mn. Since the Finite Element Model is based on Fick's diffusion for the Fe-concentration in the Al-phase, we use the differences in the solute concentration between the α and β interfaces instead. For the FEM calculations, the solubility product of the β-Al_5FeSi plate, as derived by Thermo-Calc, is expressed in an Arrhenius relation:

$$c_{\text{Fe}}^s c_{\text{Si}}^s = A_\beta \exp\left(\frac{-Q}{RT}\right) \quad (2)$$

The Thermo-Calc calculations lead to $A_\beta = 10$ and $Q_\beta = 115$ kJ/mol. Since α particles do not have a uniquely defined stoichiometry, we did not find a solubility product for the solubility at the α/Al interface. Therefore, for the FEM calculations we use the Thermo-Calc values for the α/Al interface concentrations.

3.3.1. Dependence of the interfacial concentration of Fe on the Mn content

It was found by experiment that the Mn alloy content has a large effect on the transformation speed [1,2,20,21], and therefore it is to be expected that the Mn content influences the driving force $\Delta\mu_{\text{Fe}}$ of the transformation considerably.

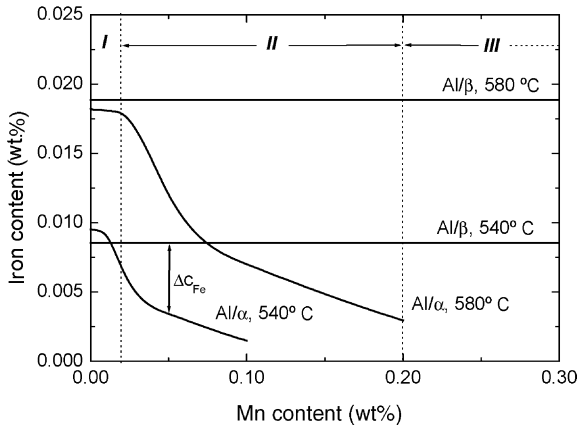

Fig. 4. Plots of the interfacial matrix concentrations (c_{Fe}) as a function of the Mn matrix content. The results were obtained by Thermo-Calc. Plots are drawn for both Al/α and Al/β interfaces, at homogenisation temperatures of 540 and 580 °C. For the presented calculations a fixed matrix concentration of 0.5 wt.% Si is used.

$\Delta\mu_{\text{Fe}}$ is approximately proportional to the logarithm of the concentration difference. Fig. 4 shows the influence of the Mn solute level in the solubility of Fe on the intermetallic interfaces at industrial temperatures of homogenisation (540 and 580 °C). As an example the concentration difference (Δc_{Fe}) between the α/Al and β/Al interface are indicated for a Mn matrix concentration of 0.05 wt.% at 540 °C.

Fig. 4 is divided into three domains indicated by region I, II and III. In domain I, representing Mn concentrations between 0 and 0.02 wt.%, the driving force Δc_{Fe} is negative or very small, and therefore the β-AlFeSi particles will not, or only slowly, transform by diffusion controlled transformation to the α-Al(FeMn)Si particles. In some parts of this domain the solubility of the α_h is lower than α_c, and in this case, the α_h is stabilised. In domain II, representing Mn alloy contents between 0.02 and 0.2, an addition of Mn increases the transformation speed considerably. In region III, with Mn concentration higher than 0.2 wt.%, the transformation speed remains high and does not significantly depends on the Mn content anymore. These qualitiative predictions are in agreement with experimental data by Zajac et al. [2].

3.3.2. Dependence of the interfacial concentration of Fe on the Si content

It is reported in the literature [1,2,16] that the transformation speed decreases as the Si level increases. Therefore, it is expected that also the Δc_{Fe} decreases with increasing Si concentration. Fig. 5 shows the influence of the Si matrix concentration on the Fe matrix concentrations at the β/Al and α/Al interfaces for $T = 540$ °C. In the calculated results a fixed matrix concentration of 0.02 wt.% Mn was used. The figure shows that the influence of the Silicon matrix concentration on the Fe solubility ranges over a wider range (0–1 wt.%) than that of Mn (0–0.2 wt.%). As expected, the driving force Δc_{Fe} decreases with the Si concentration in the matrix. This effect is indicated in the figure for two values of Δc_{Fe} at Si levels of

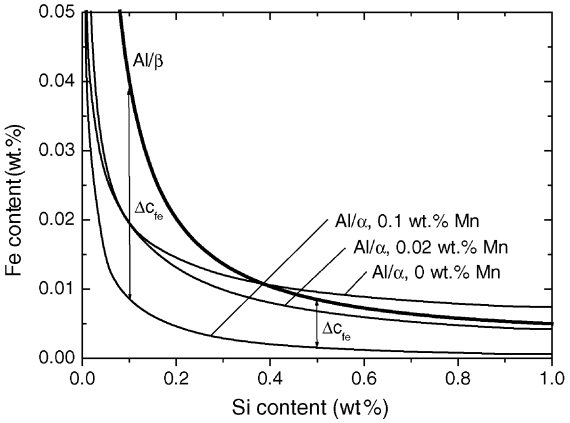

Fig. 5. The interfacial matrix concentrations (c_{Fe}) as a function of the Si matrix content. The data was obtained by Thermo-Calc. Plots are drawn for both Al/α and Al/β interfaces, for various Mn matrix compositions at a homogenisation temperature of 540 °C.

0.1 and 0.5 wt.% Si, which shows a significant drop in Δc_{Fe} for the latter case. The figure also shows that the drop of the Δc_{Fe} is larger for alloys with lower Mn contents. Therefore, it is concluded that a combination of low Mn concentration and high Si concentration leads to a very low driving force and transformation rate. For the zero Mn level, this effect is such that negative Δc_{Fe} values are obtained. In this case no phase transition of β to α will occur and annealing would only result in a growth of the β plates. Such behaviour has indeed been reported [22].

Now we investigate the combined effect of the Mn and Si matrix concentrations on the driving forces in more detail. Fig. 6 shows the iso-Δc_{Fe} contours for a window of matrix concentrations of 0–0.2 wt.% Mn and 0.2–1.0 wt.% Si levels, at a temperature of $T = 580$ °C. Each contour represents the Mn and Si concentrations for which the Δc_{Fe} is the same, and therefore are expected to have the same transformation rate.

In the figure, three different regions of matrix compositions, labelled by A, B and C, are indicated. The alloys in region A have relatively high Mn and low Si concentrations. At those compositions the Δc_{Fe} is relatively large (>0.020 wt.%), hence the transformation is fast. The alloys in region B have low Mn and high Si concentrations. At those compositions the Δc_{Fe} is relative small (<0.005 wt.%), hence the transformation is relatively slow. The alloys in region C have a very low Mn concentration and high Si concentrations. At those compositions the Δc_{Fe} is negative, and therefore the β phase is stable and a β-to-α transformation does not take place.

3.4. Kinetics

In this section, we present some calculated transformation rates as a function of time for several values of the Mn and Si content.

3.4.1. Influence of the Mn content on transformation

First, the influence of the Mn matrix content on the β-to-α transformation rate is investigated. For this case we took a fixed Si-matrix concentration of 0.3 wt.%. Fig. 7 shows the transformed fraction as a function of time of various alloy Mn levels. Mn additions between 0 and 0.02 wt.% show a small effect on the transformation rate. However, Mn additions between 0.02 and 0.20 wt.% give a considerably larger effect on the transformation rate. It was found that Mn additions larger than 0.20 wt.% have almost no extra effect on the transformation rate anymore, since in this case the maximum Fe concentration difference between the α/Al and β/Al interface is achieved according to the phase diagram as has been calculated using the database Thermo-Calc. We note here that the exactness of the phase diagram is of importance in all our calculations. Furthermore, the amount of Fe and the homogenisation temperature have a significant influence on the transformation rate.

3.4.2. Influence of Si content on transformation

Fig. 8 shows the transformed fraction as a function of time for various Si matrix concentrations. The figure shows that a variation of the Si concentration between 0.1 and 1 wt.% has a large influence on the transformation rate. Fig. 8a shows the

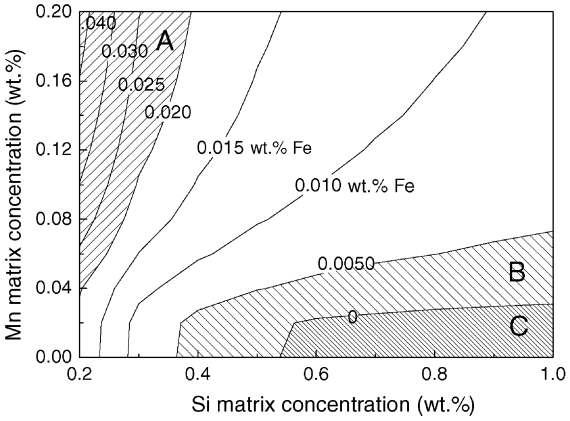

Fig. 6. Iso-Δc_{Fe} contours for a window of Mn and Si compositions.

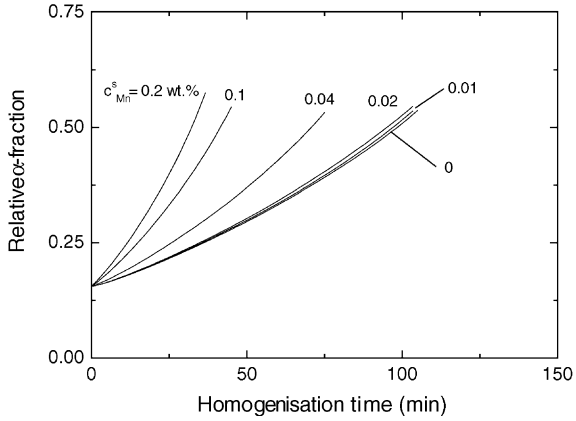

Fig. 7. Transformed fraction as a function of time at various Mn levels.

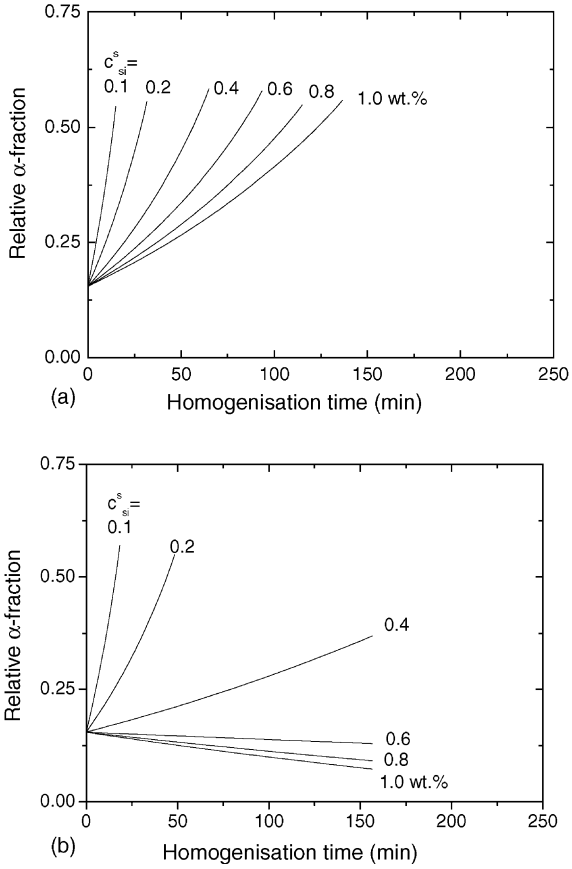

Fig. 8. Transformed fraction as a function of time at various Si levels. (a) With a fixed Mn matrix concentration of 0.10 wt.%. (b) With a fixed Mn matrix concentration of 0.02 wt.%.

influence of Si in the case of a large Mn content of 0.10 wt.%. Fig. 8b shows the influence of Si in the case of a small Mn content of 0.02 wt.%. The figure indicates that, when decreasing the Mn content, the influence of the Si content on the transformation rate increases considerably. The cases of a Si matrix concentration of 0.6, 0.8 and 1.0 wt.% in Fig. 8b are hypothetical, since in this case Δc_{Fe} is negative, and the Finite Element Model predicts that the β particles will be stabilised.

3.4.3. Influence of both Mn and Si content on transformation rate.

Now, we investigate the combined effect of the Mn and Si matrix concentrations on the transformation time. Fig. 9 shows the iso-time contours for various Mn and Si alloy contents. Each contour represents the Mn and Si content for which the transformation time up to a fraction of $f_\alpha = 0.5$ wt.% is the same. The figure indicates that the transformation time could be short (30 min), for alloys with a low Si and high Mn content. On the other hand, long homogenisation times, longer than 4 h, are required for alloys with a high Si and low Mn content. In the extreme case, of a high Si content, and a Mn content lower than 0.02 wt.%, there is no transformation anymore. The dashed area in the diagram indicates the alloy compositions in which there is no transformation.

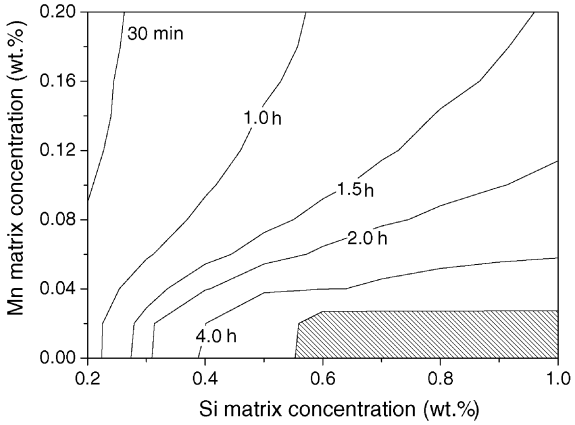

Fig. 9. Iso-transformation-time contours for a window of Mn and Si compostions.

4. Experimental

For our experiments we prepared two sets of samples. The first set is designed to study the effect of the Mn contents on the β-to-α transformation rate. The second set is designed to study the combined effect of the Mn and Si content on the temperature dependence of the β-to-α transformation.

For the first set of samples we used three different Al–Mg–Si alloys, all with a concentration of ∼0.4 wt.% Mg, ∼0.6 wt.% Si and ∼0.2 wt.% Fe similar to those in an AA 6063 alloy. The Mn concentration was varied between 0.01 and 0.05 wt.%. Table 2 presents the exact compositions of the alloys, labelled by H1, H2 and H3, with a low, medium and high Mn content, respectively. Samples of each alloy were homogenised at a fixed temperature of 580 °C for times ranging between 10 min and 2 days.

For the second set of alloys we used two types, AA 6063 and AA 6005A alloy, labeled as A1 and A2, respectively. Both alloys differ mainly in Si and Mn content. Table 3 presents the exact compositions of the alloys, as determined by chemical

Table 2
Alloy compositions (wt.%) of first set of samples, used for the investigations of the effect of the Mn content on the β-to-α transformation rate

Alloy	Mn	Si	Fe	Mg	Other
H1	0.011	0.61	0.20	0.43	≤0.02
H2	0.022	0.64	0.23	0.43	≤0.02
H3	0.044	0.63	0.22	0.44	≤0.02

Table 3
Alloy compositions (wt.%) of second set of samples, used for the investigation of temperature-dependence of the β-to-α transformation

Alloy	Mn	Si	Fe	Mg	Other
A1	0.02	0.58	0.18	0.43	≤0.03
A2	0.18	0.83	0.27	0.70	≤0.02

analysis. Alloy A1 has a low Si and Mn content, whereas alloy A2 has a high Si and Mn content. Series of samples of each alloy were homogenised at temperatures ranging from 540 to 590 °C for times between 15 min and 4 days.

Both sets of samples were taken at locations between 10 and 30 mm from the rim of the original DC-cast billets, which had a diameter of 203 mm (H1, H2, H3 and A1) or 254 mm (A2). The microstructures of these samples, represent the typical microstructure of the billet. For the homogenisation of the samples we used an air circulation oven, for which the maximum temperature deviation over all locations in the oven was 3 K for ΔT. The samples were ground and polished down to 1/4 μm silica, where the polishing plane is taken parallel to the surface of the billet. The relative α-fraction was determined using automatic SEM measurements in combination with electron dispersive X-ray spectometry (EDX). The α and β particles were classified on the basis of the (Fe + Mn)/Si ratios. The method is described in more detail in [6].

To verify whether the initial microstructures of all alloys were comparable, we determined the dendrite arm spacing (DAS) and the thickness of the β plates in each alloys. The DAS of each cast alloy was determined by averaging 40 separate spacings from 5 optical micrographs on the same polished sample. Comparable DAS values ranging from 18 to 20 μm with standard deviations of 4 μm were obtained. The thickness of the β plates was obtained by SEM observations with a JEOL 5600F at a voltage of 2 keV. For each alloy we investigate samples, which were homogenised for 30 min at 580 °C. For this homogenisation time, the Mg_2Si particles had dissolved while the β-intermetallics dimensions were practically not affected. Each sample was prepared and polished as described before and subsequently electro-etched at 20 V during 30 s in a mixture of 78 perchloric acid, 90 ml water, 730 ml ethanol and 100 ml butylglycol. The apparent thickness d' as observable in 2D cross sectional images was determined by averaging the thickness of 50 β-plates, using the area's of the particles as weight factors of the determination of the mean. The true thickness d was obtained using $d = (\pi d'/4)$. The corrected thickness varied between 0.2 and 0.3 μm with a large natural standard deviation of 0.05 μm. The thickness distributions all had a median at around 0.2 μm. The small differences in the DAS value and β plates thickness between the various alloys confirmed that the initial microstructures of all alloys under investigation are comparable.

The nucleation distance is an important input parameter in the FEM and therefore this was determined for each alloy separately. The nucleation distance between individual α particles was measured on fully homogenised samples (2 days at 580 °C). After this homogenisation, the intermetallics are present as strings of α particles. On average, one string contained approximately four or five α particles. The α particles situated on one string were formerly nucleated on the faces of one β plates. Therefore, the distances between those transformed α particles represents the initially nucleation distance on the β plates. Twenty optical micrographs were made on each polished sample. The nucleation distance was obtained by $l' = L/(n-1)$, where L represents the distance between the outside particles, and n is the number of particles which are present in a sequence. The average nucleation distance in the polished plane was determined by averaging the results of 20 strings of α-particles. Subsequently we made a correction for the translation to the average nucleation distance in 3D morphology by $l = l'/2$.

5. Results and discussion

5.1. Influence of the Mn level on transformation

Fig. 10 presents the measured fraction transformed as a function of homogenisation time for various alloys with Mn concentrations ranging between $c_{Mn} = \sim 0.01$ and 0.2 wt.% on material that was homogenised at 580 °C. As expected, the rate of transformation increases significantly as the Mn alloy concentration increases. The transformation rate shifts by almost two decades when going from the low Mn alloy ($c_{Mn} = 0.01$) to the Mn rich alloy ($c_{Mn} = 0.2$). From the figure, the experimental transformation rates at $f_\alpha = 0.25$ and $f_\alpha = 0.50$ can be determined for comparison with the rates predicted by use of the model. The experimental rate of the transformation is determined by the derivative in time of the f_α fraction (df_α/dt).

Considering the model, it is expected that, when the temperature is constant, the rate of the transformation is almost linear with the difference of the Fe concentration at the α and β interface (Δc). For a general representation of the results, we define the "kinetic force" by $D\,\Delta c$. In this case the temperature is constant and hence the diffusion coefficient does not change. To test whether this linear behaviour also holds for our experimental rates, we plot the experimental and modelled rates as a function of $D\,\Delta c$ for $f_\alpha = 0.25$ and $f_\alpha = 0.5$ in Fig. 11a and b, respectively.

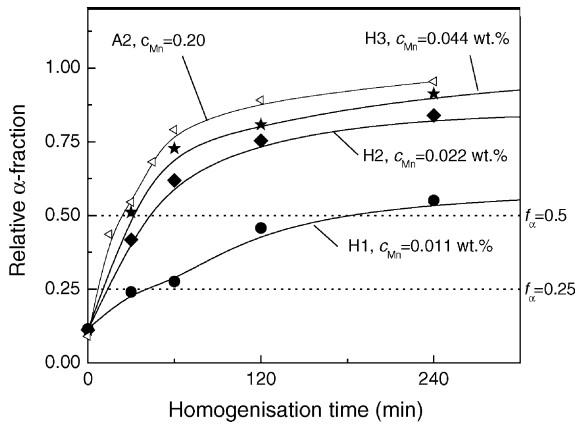

Fig. 10. Measured transformation fraction at 580 °C for alloys containing various Mn levels. The labels of the alloys and the Mn contents of the various alloys are indicated in the figure.

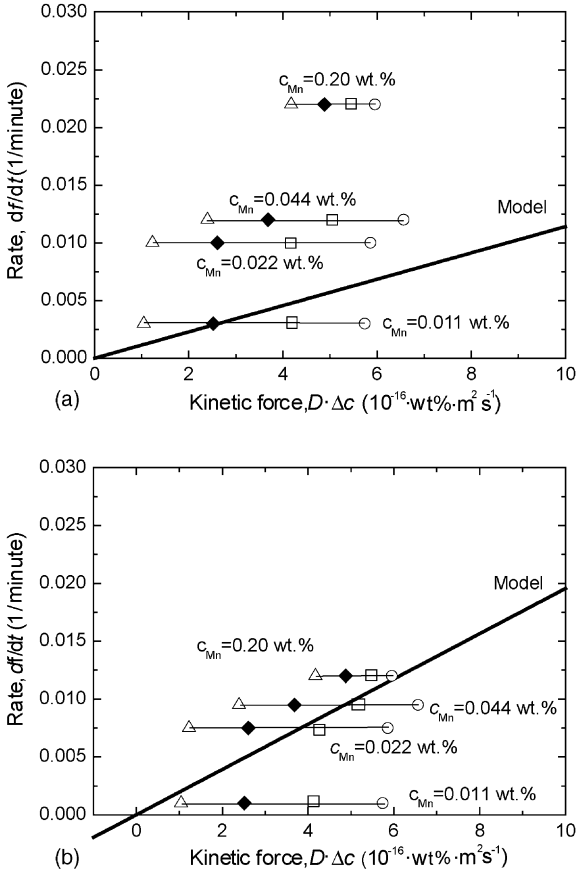

Fig. 11. Measured transformation rate versus determined kinetic force, $D\,\Delta c$, compared with model. (a) For $f_\alpha = 0.25$; (b) for $f_\alpha = 0.5$; (△, ◆, □, ◯): measured rates at various kinetic forces as derived for the bounded silicon concentrations $\Delta c_{Si} = 0.2$, 0.3, 0.35 and 0.4 wt.%; (—) model.

In calculating the kinetic force, it was assumed that part of the Si concentration (Δc_{Si}) is bound to precipitates and intermetallics, and giving reduction of the Si matrix concentration by: $c_{Si\,matrix} = c_{Si\,alloy} - \Delta c_{Si}$. Therefore, Fig. 11 shows for four experimental alloys the rate of transformation as a function of the calculated kinetic force for various Δc_{Si} values, ranging between 0.2 and 0.4 wt.%. The solid lines give the predicted rate as a function of kinetic force, showing, as expected, a linear behaviour.

Fig. 11b shows that for the experimental rate at $f_\alpha = 0.5$ the experimental transformation rate are comparable with the model prediction at a Si binding of $\Delta c_{Si} = 0.35$. The rate at low Mn level of 0.011 wt.% deviates from this trend. One explanation for the anomalously low speed for low Mn alloys is that now hexagonal α particles are formed, which might have a different growth mechanism [2]. Another explanation is that the low Mn content leads to a less cubic α nuclei, leading to a slower transformation.

Fig. 11a shows that the experimental rate at $f_\alpha = 0.25$ deviates significantly from the model. Possibly this is due to the uncertainty in the initial α particle size and incubation time.

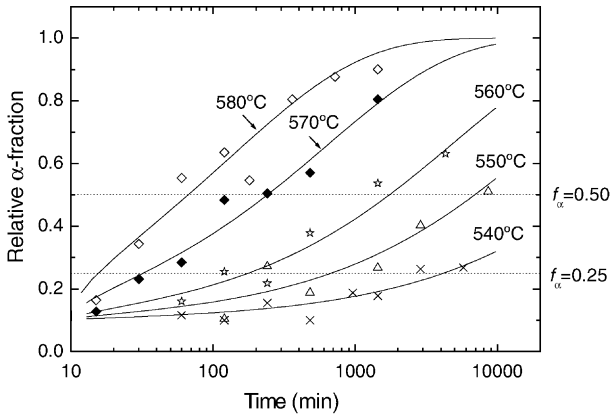

Fig. 12. The relative α-fraction of a 6063 alloy with a low Mn and Si content as a function of time for several temperatures: (◊) 580 °C; (◆) 570 °C; (☆) 560 °C; (△) 550 °C; (×) 540 °C. The trends of the measured temperature are indicated in the graph by the solid lines.

5.2. Influence of alloy contents on T-dependence of transformation

Fig. 12 shows the kinetics at various temperature for an AA 6063 alloy (alloy A1), which has a low Mn alloy content of 0.02 wt.%. The Johnson–Mehl–Avrami equation [23], $f_\alpha = 1 - \exp(1 - kt^n)$ was used to fit the experimental data points. It was found that for all temperatures the parameter n was approximately 0.5, which is in line with a diffusion controlled transformation [23]. Fig. 12 makes it clear that the transformation in the AA 6063 alloy has a strong temperature dependence. The figure shows that for a homogenisation temperature of 540 °C there is hardly any transformation, even after homogenisation times of 5760 min (4 days), whilst for a homogenisation temperature of 580 °C, the material is already homogenised to a fraction of $f_\alpha = 0.8$ after 360 min (6 h). The temperature dependence of the transformation in an AA 6005A alloy [7] (alloy A2), which had a higher Mn and Si content, was found to be less than that for the AA 6063 alloy.

In Fig. 13, the experimental transformation rates at $f_\alpha = 0.25$ and $f_\alpha = 0.50$ are compared with the rates predicted by our model, for alloys which have a low (0.02 wt.%) and a high (0.18 wt.%) Mn content. For the model we used a bounded Si concentration of $\Delta c_{Si} = 0.35$. Again, the experimental rate was determined by the derivative with respect to time of the f_α fraction (df_α/dt). Since the transformation rate decreases as time proceeds in our experiments, the experimental transformation rate at $f_\alpha = 0.25$ is higher than at $f_\alpha = 0.5$. From the model we observe the contrary; since the modelled transformation rate increases during time, the modelled rate at $f_\alpha = 0.25$ is lower than at $f_\alpha = 0.5$. Probably this is due to the model assumption that the interfacial concentrations are fixed at all times during the transformation process. Multi-component models show that the interfacial concentration changes as time proceeds (see [7]). The assumption of fixed interfacial concentrations is used

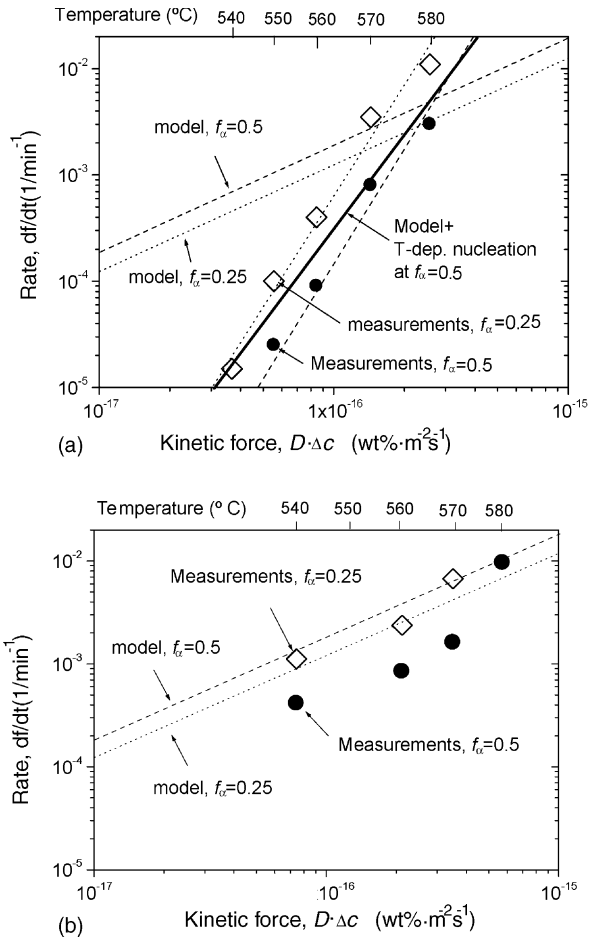

Fig. 13. Measured and modelled transformation rates versus the theoretical kinetic force, $D\,\Delta c$. (a) For an alloy with a low Mn content (alloy A1). (b) For an alloy with a high Mn content (alloy A2). The corresponding temperatures are indicated on the top-axis. The dotted and dashed lines indicate the trends at $f_\alpha = 0.25$ and at $f_\alpha = 0.5$, respectively. The straight line in (a) indicates the model results at $f_\alpha = 0.5$ in the hypothetical case of a temperature dependence in nucleation distance.

here since multi-component effects have not yet been implemented in the Finite Element Model. This will serve as an accurate approximation for the early stages of the transformation.

From the model, it is expected that the transformation rate at a certain transformed fraction is linear with the diffusion coefficient and the Fe concentration difference between the β/Al and α/Al interface. From Fig. 13 it is clear that for the model calculation, the rate is indeed linear with the kinetic force. For the model calculations at all temperatures we used the geometrical parameters as determined experimentally at 580 °C.

Fig. 13a shows that the temperature dependence of the experiments with a low Mn alloy composition is different from the model predictions. The model calculations in Fig. 13a show that the rate depends on the kinetic force according to a power law, but the slope of the measurements differs significantly from the slope obtained by the model predictions. In contrast, Fig. 13b shows that the temperature dependence of the experiments for high Mn concentrations (alloy A2) agrees better with the model predictions. The experimental rates have an almost linear relation with the kinetic force and the experimental fractions at $f_\alpha = 0.25$ show an almost perfect match with the model (see Fig. 13b).

Although a perfect agreement between the model and the measurements is not to be expected due to the many simplifications in the model, the very big difference in activation energy (Q_{exp} = 950 kJ/mol versus Q_{FEM} = 300 kJ/mol) for the alloy with a low Mn content (see Fig. 13a) is rather surprising. When we examine the temperature dependence of parameters in the model, only the diffusion coefficient and the Δc_{Fe} are taken to be *T*-dependent while all geometrical factors are fixed. This assumption is probably incorrect for the nucleation distance must be *T*-dependent [24]. Unfortunately we did not succeed in determining it experimentally. However, we can use the model to explore the effect of a temperature dependent nucleation distance on the transformation rate. If we assume that at 540 °C the nucleation distance is 7 times longer as that at 580 °C, we get a better agreement between the apparent model predictions and the experimental data (see solid line in Fig. 13a). In this case, the experimental activation energy becomes close to the modelled apparent activation energy ($Q_{apparent}$ = 900 kJ/mol). This apparent activation energy is equal to the addition of the activation energy of diffusion (Q = 183 kJ/mol), the activation energy of Δc_{Fe} (Q = ∼120 kJ/mol) and the activation energy of nucleation (Q = ∼600 kJ/mol). In contrast, for the alloy with a high Mn content the experimental activation energy (Q_{exp} = 370 kJ/mol) was found to be close to the modelled activation energy (Q_{FEM} = 300 kJ/mol). This might suggest that for alloys with high Mn contents the nucleation activation energy is low (Q = ∼70 kJ/mol), and therefore the nucleation distances are only slightly *T*-dependent.

An other possible cause for the gap between the experimental and modelled transformation rates for alloys with a low Mn content is the fact that multi-component effects at the α-interface were not taken into account sufficiently. Since, the displacement of the α-interface should be equal for all alloying elements that are in the α-particle, this poses an additional requirement on the relation between the interface concentrations of Mn and Fe. An estimate can be obtained by the use of the methods in [7]. Due to low sensitivity of the Fe interfacial concentration for high Mn interfacial concentrations, this effect was not so important for the determination of the interface concentration in alloy A2, where only high Mn levels were considered. However, in the configuration where the Mn contents may be low, the multi-component effects may be more pronounced.

5.3. Industrial implications

A proper homogenisation leads to a considerable increase of the extrudability and to fewer surface defects

on the aluminium profiles. Therefore, preferably an extrusion ingot is homogenised to attain a high relative α fraction, e.g. at least $f_\alpha = 0.8$ and preferably more than $f_\alpha = 0.9$ [1]. Although the presented transformation model is not applicable to homogenisation up to high relative α-fractions, yet still some important implications for the alloy compositional dependence of the homogenisation kinetics can already be extracted from the numerical experiments.

Mg is added to the AA 6xxx alloys system to form the age hardable Mg–Si precipitates in the final extrusion product. However, since Mg has practically no influence on the interfacial concentrations on the β and α particles [15], this element has almost no influence on the transformation rate.

The Fe alloy content has some influence on the transformation speed since it influences the morphology of the cast β-AlFeSi particles. In AA 6xxx alloys, almost all the Fe in the alloy system will bind with the excess of Si and the abundant Al to form the β-intermetallics. Therefore, alloys with a low Fe concentration are preferable since after casting less β-intermetallic volume is formed and probably this leads to thinner β-plates, which leads to a faster β-to-α transformation. Note that the Fe alloy content has hardly any influence on the Fe interfacial concentration of the β and α particles itself.

The Si content has a modest influence on the transformation rate. It appears that the Si matrix concentration has an effect on the Fe interfacial concentration of the β and α particles. Since only a small part of the Si alloy content binds to the β-AlFeSi particles, it can be assumed that the Si matrix concentration is approximately equal to the Si alloy content. It was found in the model that a low alloy Si content (e.g, <0.5 wt.%) is preferable since this leads to a faster β-to-α transformation.

Of all alloying elements the Mn alloy content has the largest influence on the transformation rate. As it strongly affects the thermodynamic potential difference of the rate determing element Fe at the interfaces between the matrix at the β particle and the matrix at the α particle. A low Mn concentration of 0.01 wt.% leads to a very slow transformation rate or even to no transformation. It was found that small alloying additions of up to 0.2 wt.% Mn gives a large increase in the transformation rate. Finally our transformation model tells us that larger Mn additions in excess of 0.2 wt.% will give no significant extra increase of the transformation rate anymore. Therefore, for industrial purposes, a Mn content of approximately 0.2 wt.% is optimal for the transformation speed. Mn additions higher than 0.2 wt.% might only be useful for other alloying purposes, such as the formation of more dispersiods inside the Al-matrix.

From the experiments we conclude that the transformation rate for alloys with low Mn content (e.g., ∼0.02 wt.% Mn) are highly temperature dependent. Therefore, for low Mn alloyed alloys, extra care for accurate temperature control is an important aspect to achieve a guaranteed level of transformation.

6. Conclusions

The Finite Element Model, as presented in [7], was used to describe the influence of the alloy content on the β-to-α transformation rate. Thermodynamic databases (Thermo-Calc) were used to derive the Fe interfacial concentrations at the interfaces of both the α and β intermetallics for several alloy compositions. The model predicts a significant effect of the Si and Mn alloy content on the transformation kinetics. It was found that Mn has the largest effect on the transformation rate. The results of the model correspond with trends found with experiments both presented in this paper and observed by other authors. We conclude from this agreement that it is justified to use the hypothesis that the driving force of the transformation is the difference in Fe concentration at the Al-α and Al-β phase interfaces.

References

[1] N.C. Parson, J.D. Hankin, K.P. Hicklin, US Patent 6,440,359 (2002).
[2] S. Zajac, B. Hutchinson, A. Johansson, L.O. Gullman, Mater. Sci. Tech. 10 (1994) 323–333.
[3] A. Valles, R.P.L. Orsetti, I. Diaz, R. Tosta, in: T. Sato, S. Kumai, T. Kobayashi, Y. Murakami (Eds.), Proceedings of the Sixth International Conference on Aluminium Alloys, Toyohashi, Japan, 1998, pp. 2123–2128.
[4] N.C.W. Kuijpers, J. Tirel, D.N. Hanlon, S. van der Zwaag, Mater. Char. 48 (2002) 379–392.
[5] T. Minoda, H. Hayakawa, H. Yoshida, Mater. Sci. Technol. 7 (2000) 13–17.
[6] N.C.W. Kuijpers, W.H. Kool, P.T.G. Koenis, K.E. Nilsen, I. Todd, S. van der Zwaag, Mater. Char. 49 (2002) 409–420.
[7] N.C.W. Kuijpers, F. Vermolen, C. Vuik, S.vd. Zwaag, Mater. Trans. 44 (2003) 1448–1456.
[8] L.F. Mondolfo, Structure and Properties of Aluminium Alloys, Butterworth, London, England, 1976.
[9] L. Bäckerud, Jernkont. Ann. 152 (1968) 109–138.
[10] F.J. Vermolen, C. Vuik, Comput. Appl. Math. 126 (2000) 233–254.
[11] H.W.L. Phillips, Annotated Equilibrium Diagrams of Some Aluminium Alloy Systems, The Institute of Metals, London, 1959.
[12] V. Stefániay, A. Griger, T. Turmezey, J. Mater. Sci. 22 (1987) 539–546.
[13] A.L. Dons, Z. Metallkd. 77 (1986) 126–130.
[14] A.L. Dons, Z. Metallkd. 76 (1985) 609–612.
[15] P. Kolby, in: T.H. Sanders, E.A. Starke Jr. (Eds.), Proceedings of The Fourth International Conference on Aluminium Alloys, Georgia Institute of Technology, School of Materials Science and Engineering, Atlanta, 1994, pp. 2–17.
[16] Y. Langsrud, Key Eng. Mater. 44–45 (1990) 95–116.
[17] J.E. Tibballs, J.A. Horst, C.J. Simensen, J. Mater. Sci. 36 (2001) 937–941.
[18] G. Segal, C. Vuik, F.J. Vermolen, J. Comp. Phys. 141 (1998) 1–21.

[19] D.L. Beke, I. Gödény, I.A. Szabó, G. Erdélyi, F.J. Kedves, Philos. Mag. A5 (1987) 425–443.
[20] H.J. Lamb, Proceedings of the Conference on Phase Transformations, Series 3, The Institution of Metallurgists London England, 1979, pp. V4–V5.
[21] M. Ryvola, L.R. Morris, Microstruct. Sci. 5 (1977) 203–208.
[22] N.A. Belov, A.A. Aksenov, D.G. Eskin, in: J.N. Fridlyander, D.G. Eskin (Eds.), Iron in Aluminum Alloys, Impurity and Alloying Element, Taylor & Francis, London, 2002, pp. 132–136.
[23] J.W. Christian, The Theory of Transformations in Metals and Alloys, Pergamon Press, Oxford, 1965.
[24] D.A. Porter, K.E. Easterling, Phase Transformations in Metals and Alloys, Chapman & Hall, London, 1997.